RSC Advances

ROYAL SOCIETY OF CHEMISTRY

www.rsc.org/advances

Table of Contents Entry

Rutile nanorods are grown on the anatase nanotubes to enhance the photocurrent density in photocatalytic water splitting.

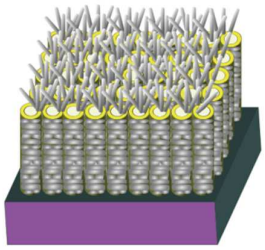

Hybrid nanostructures of mixed-phase TiO_2 for enhanced photoelectrochemical water splitting

Wenbin Huang,[*a] Xuyue Wang,[a] Yali Xue,[a] Yang Yang,[a] and Xianyu Ao[*a]

Abstract: Mixed-phase TiO_2 nanostructures are synthesized by hydrothermal treatment of anodized TiO_2 nanotubes. The growth of rutile nanorods on the anatase nanotubes can greatly expedite the electron-hole separation and transportation, enhance the light absorption, and also increase the surface area. When used for photocatalytic water splitting, more than three-fold enhancement in photocurrent density is observed for mixed-phase TiO_2 nanostructures, relative to pristine TiO_2 nanotubes.

Introduction

Photocatalytic splitting of water into H_2 is a potential solution for sustainable energy. When a semiconductor is irradiated with sunlight, the electrons in the valence band are promoted to the conduction band, leaving positively charged holes in the valence band. These photo-generated electrons and holes drive the reduction and oxidation reactions in the photocatalytic water splitting. Among various photoanode materials, TiO_2 distinguishes itself due to its favorable band-edge positions, high resistance to photocorrosion, non-toxicity and low cost.[1] For semiconductor metal oxides, however, only a small fraction of the holes (when used as photoanodes) can reach the semiconductor/electrolyte interface, since most of the photo-generated charge pairs recombine either radiatively or non-radiatively. Apart from the short lifetime of charge carriers, the light absorption efficiency of metal oxides is also quite low. Besides the efforts in optimizing the material itself[2-5] (e.g., sensitizing with small band gap semiconductors/dyes,[6-8] doping with metal and non-metal,[9-14] or partially reduction[15,16] to extend the absorption from UV to visible region), it is also promising to increase the optical path length while keep the charge carrier

transport distance short. This can be accomplished in nano-rod/tube arrays or other nanostructures with large surface-to-volume ratios.[17-30] On the other hand, TiO_2 nanostructures consisting of rutile and anatase phases have been demonstrated with enhanced photocatalysis efficiency,[31-43] however, most reports on the mixed-phase TiO_2 were based on Degussa P25[31-33] or nanoparticles.[36-40,42] Previously Lin *et al.* reported the synthesis of rutile TiO_2 nanostructures on anatase nanotubes with $TiCl_3$ as the precursor for DSSC,[34] but their rutile TiO_2 rods were short and small due to the low temperature and low pressure environment used.[26]

Here we report a kind of hybrid TiO_2 nanostructures for photoelectrochemical (PEC) water splitting, consisting of rutile TiO_2 nanorods synthesized by hydrothermal method on anodized TiO_2 nanotubes in a high temperature and high pressure condition with titanium isopropoxide as the reaction precursor. We find that both the Ti foil and the TiO_2 nanotubes are dissolved if we use $TiCl_3$ as the precursor at 150℃. This kind of hybrid nanostructures has better charge transport and light absorption properties than pristine nanotubes or nanorods due to the combining of anatase phase and rutile phase. We observed more than three-fold enhancement in photocurrent density relative to pristine TiO_2 nanotubes.

Experimental

Preparation of TiO_2 nanotubes: Highly ordered TiO_2 nanotube arrays were fabricated by two-step anodization of Ti foil (99.4% purity, Alfa Aesar) in a two-electrode cell with platinum gauze as the counter electrode under constant current at room temperature. The electrolyte contains 0.5 wt% NH_4F and 2 vol% H_2O in ethylene glycol. In the first-step anodization, a current density of 20 mA/cm^2 was applied for 60 min, and then the anodized layer was removed by ultrasonic in DI water. After that, the Ti foil was subjected to a second anodization for 20 min, and then cleaned with DI water and dried with nitrogen

stream. Finally, the Ti foil was annealed in air at 500℃ for 2 hours with a heating rate of 4℃/min to transform amorphous TiO_2 into crystalline.

Formation of hybrid TiO_2 nanostructures: In a typical synthesis, 0.24 ml titanium isopropoxide was added into 20 ml of HCl aqueous solution (10 ml DI water mixed with 10 ml 38 wt% HCl) under magnetic stirring. After stirring for another 5 min, the solution was poured into a Teflon-lined stainless steel autoclave (50 ml volume), and then the annealed Ti foils were transferred into the autoclave for hydrothermal treatment at 150℃ for 3~9 h in an oven. The autoclave was then cooled down to room temperature under flowing water. The samples were taken out and rinsed with DI water and blown dry with nitrogen, then annealed in air at 500℃ for 1 hours with a heating rate of 4℃/min.

Characterization: The crystal structure of the prepared TiO_2 nanostructures was examined by X-ray diffraction (XRD, Bruker D8 Advance). Morphological and lattice structural information were examined with field emission scanning electron microscopy (SEM, Zeiss Ultra 55) and transmission electron microscopy (TEM/HRTEM, JEM-2100HR). Photoluminescence (PL) spectrum was measured under an inverted optical microscope (Olympus IX81) equipped with a mercury lamp, a band pass filter (330-385 nm) for excitation, and a long pass filter (420 nm) for emission, together with a spectrometer (Ocean Optics QE65000 Pro). Reflection was measured by a spectrophotometer (Perkin Elmer Lambda 950) with a 150 mm integrating sphere.

Photoelectrochemical measurements: The PEC performance was evaluated by a potentiostat (CHI 660D) in a three-electrode cell with TiO_2 as the working electrode, Ag/AgCl as the reference electrode, and Pt as the counter electrode. The supporting electrolyte was 1 M KOH solution. The potential is reported against the reversible hydrogen electrode (RHE) following the equation below:

$$E_{RHE} = E_{Ag/AgCl} + 0.059\ pH + E^{0}_{Ag/AgCl},$$

where $E^{0}_{Ag/AgCl}$ = 0.1976 V at 25℃. The scan rate for the linear sweep voltammetry was 10 mV/s. The photocurrent was measured under irradiation

from a Class AAA solar simulator (Newport 94023A) which was used to simulate AM 1.5G illumination and the intensity of the light source was calibrated with a Si reference cell (Newport 91150V). The IPCE was measured by using a monochromator (Newport QEPVSI-b) together with CHI 660D at 0.23 V *vs* Ag/AgCl.

Results and discussion

The hybrid TiO_2 nanostructures were synthesized by a hydrothermal method with TiO_2 nanotubes as starting substrates (Fig. 1a). TiO_2 nanotubes were obtained via two-step anodization followed by annealing in air at 500℃ for 2 h to transform amorphous TiO_2 into crystalline (at the same time an oxide was grown to protect the underlying titanium foil). As shown in Fig. 1b, the as-prepared nanotube arrays have a length of around 5 μm and diameter of around 100 nm (under 20 mA/cm^2 for 20 min). We chose constant current mode during anodization, since the diameter of nanotubes is determined by the density of electrons,[44] and the density of electrons provided by constant current mode is more stable so that the size of tubes obtained by constant current mode is more uniform than by constant voltage mode.[45] After hydrothermal treatment in a sealed environment at 150□ for 8 h,[26] a layer of TiO_2 nanorods was grown on the top of TiO_2 nanotubes (Fig. 1c). Also note that the surface of tube walls was changed from smooth to rough. We tried low temperature and pressure conditions but only got some short and stumpy nanorods. We also tried to use titanium butoxide and $TiCl_3$ as the precursor in the hydrothermal reaction at 150℃, but found that both the Ti foil and the TiO_2 nanotubes were dissolved. The success with titanium isopropoxide is probably due to the milder environment it creates, so that the superficial TiO_2 can protect the Ti sheet from corrosion.

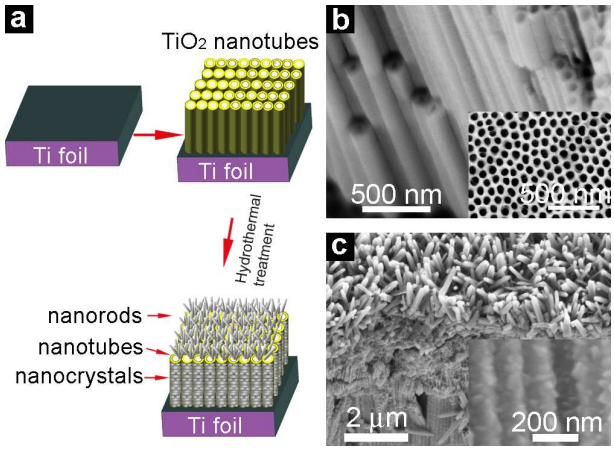

Fig. 1 (a) Schematic description of the synthesis of the hybrid TiO_2 nanostructures, consisting of an underlying layer of TiO_2 nanotubes (with nanocrystals on the tube walls) and a top layer of TiO_2 nanorods, obtained via two-step anodization followed by hydrothermal treatment. (b) Typical SEM image of TiO_2 nanotubes obtained via two-step constant-current anodization. The inset is the top view. (c) Typical SEM image of the hybrid TiO_2 nanostructures. The inset is a magnified view showing rough tube walls.

Fig. 2 displays the XRD patterns of pristine TiO_2 nanotubes and hybrid TiO_2 nanostructures after hydrothermal treatment. All diffraction peaks of TiO_2 nanotubes agree well with anatase phase, and show a strong preferential orientation of (101) ($2\theta = 25.367$). The diffraction peaks of (110) ($2\theta = 27.492$), (101) ($2\theta = 36.15$), (200) ($2\theta = 39.272$), and (211) ($2\theta = 54.435$) appeared after hydrothermal treatment agree well with typical tetragonal rutile phase.

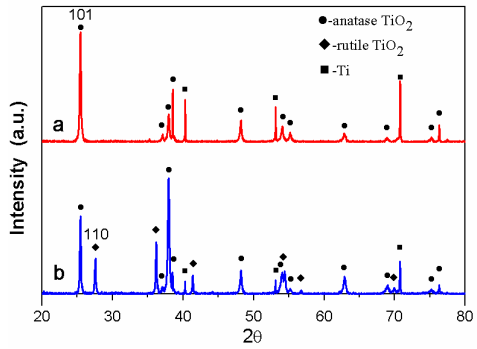

Fig. 2 XRD patterns of (a) pristine TiO_2 nanotubes and (b) hybrid TiO_2 nanostructures.

The morphology and crystalline structure of the hybrid TiO_2 nanostructures were further characterized by high-resolution TEM. As shown in Fig. 3a, the diameter of nanotubes is around 100 nm, and some nanocrystals can be identified on the tube walls. Fig. 3c indicates the polycrystalline nature of the nanotubes. The well-resolved lattice fringes of 0.352 nm seen from the HRTEM and SAED image coincide with the (101) plane of the anatase phase. Fig. 3b shows that the diameter of nanorods obtained after 6 h hydrothermal reaction was around 50 nm. Fig. 3d shows that the nanorods are monocrystalline rutile TiO_2. Combining the result of XRD, we conclude that the hybrid TiO_2 nanostructures are consisting of the anatase nanotubes and rutile nanorods.

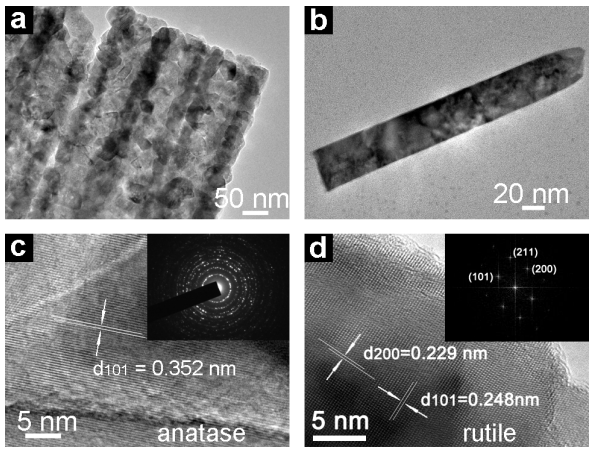

Fig. 3 TEM images of hybrid TiO_2 nanostructures obtained after hydrothermal treatment. (a) Nanotubes with nanocrystals on the wall. (b) A nanorod. (c) HRTEM image and electron diffraction pattern (inset) of a nanotube; (d) HRTEM image and FFT diffraction pattern (inset) of a nanorod.

We then study the influence of hydrothermal reaction time on the morphology of the hierarchical structures. As is shown in Fig. 4a and 4b, only sparse nanorods with the length and diameter of around 400 nm and 20 nm, respectively, were grown on the nanotubes after hydrothermal reaction for 3 h at 150℃. Both the length and the diameter of nanorods get larger as the

hydrothermal reaction time increasing. After 9 h hydrothermal reaction, the average length and diameter of nanorods can reach 1 μm and 80 nm, respectively. The nanorods are so dense that the underlying nanotubes were covered completely (Fig. 4c and 4d). Reflection measurements in visible region (data not shown) reveal that the hybrid TiO_2 nanostructures have lower reflectance than that of pristine nanotubes, and for the hybrid TiO_2 nanostructures the reflectance gets smaller with elongated hydrothermal treatment time. The nanorods behave as a gradient refractive index layer, and the combining of nanotubes with nanorods can enhance light scattering and trapping, such that the hybrid TiO_2 nanostructures have better light harvesting capability.

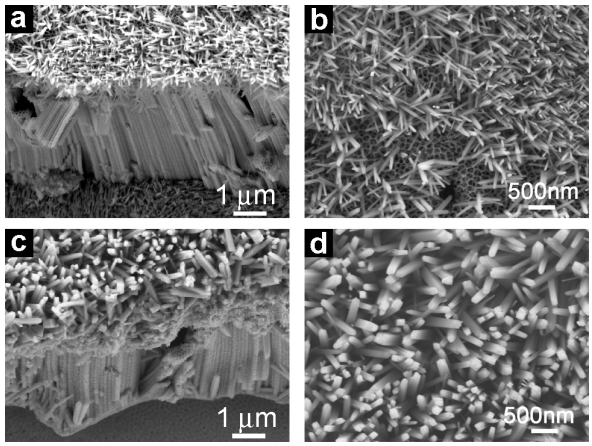

Fig. 4 SEM images of hybrid TiO_2 nanostructures with different hydrothermal reaction time, (a, b) 3 h and (c, d) 9 h. The left column and the right column shows the cross-sectional view and the top view of the sample respectively.

Fig. 5a shows typical plots of the photocurrent density versus the applied potential for TiO_2 nanotubes and hybrid TiO_2 nanostructures with different hydrothermal treatment time. All the hybrid TiO_2 nanostructures after hydrothermal treatment exhibit consistently higher photocurrent densities than pristine TiO_2 nanotubes under the same condition, indicating that the combining of anatase TiO_2 and rutile TiO_2 nanostructures can enhance the PEC

activity. As the hydrothermal reaction time increases, the nanorods grow denser, and the photo-generated current increases significantly. The photocurrent density was highest for 7 h hydrothermal reaction. However, if we increased the hydrothermal reaction time further, the photocurrent densities decreased, and the possible reason is that the layer of nanorods is too thick and dense, such that the bottom TiO_2 nanotubes do not absorb enough UV light and the conductivity decreases. The photocurrent density of the TiO_2 nanotubes is only 0.16 mA/cm^2 at 1.23 V *vs* RHE, while it is 0.71 mA/cm^2 for the hybrid structure after 7 h hydrothermal treatment.

The applied bias photon-to-current efficiency (ABPE) of two kinds of photoanodes were also evaluated. The ABPE of the can be calculated using the following equation,[27]

$$\text{ABPE (\%)} = I(E^0_{rev} - V)/J_{light},$$

where I is the photocurrent density (mA/cm^2), J_{light} is the irradiance intensity of 100 mW/cm^2, E^0_{rev} is the standard reversible potential *vs* RHE, and V is the applied potential *vs* RHE. Fig. 5b presents the ABPE plots of pristine TiO_2 nanotubes and hybrid TiO_2 nanostructures. The pristine TiO_2 nanotubes show a maximum conversion efficiency of 0.11% at 0.44 V *vs* RHE while the hybrid TiO_2 nanostructures after 6 h hydrothermal reaction exhibit a maximum conversion efficiency of 0.45% at 0.5 V *vs* RHE.

To understand the interrelation between the PEC activity and the light absorption of two types of TiO_2 structures, the incident photo-to-current conversion efficiency (IPCE) was measured at 0.23V *vs* $V_{Ag/AgCl}$ and shown in Fig. 5c. IPCE can be expressed by the equation,

$$\text{IPCE} = (1240\, I)/(\lambda J_{light}),$$

where I is the measured photocurrent density at a specific wavelength, λ is the wavelength of the incident light, and J_{light} is the irradiance intensity at a specific

wavelength. Compared with the pristine TiO_2 nanotubes, the hybrid TiO_2 nanostructures achieve much higher photoactivity over the entire UV region and reaches IPCE values of around 45% in a broad wavelength range. Also note that the hybrid nanostructures extend the photoactive range from ~ 390 nm of the pristine TiO_2 nanotubes (corresponding to the band gap 3.2 eV of the anatase phase), into the visible at ~ 410 nm (corresponding to the band gap 3.0 eV of the rutile phase).

We attribute the higher photoactivity of hybrid TiO_2 nanostructures in large part to the synergistic activation of the mixed phases of rutile and anatase,[31-33,46] and also the enhancement in light harvesting by the hybrid nanostructures. The rutile phase extends the photoactivity into the visible region, and the growth of rutile nanorods/nanocrystals on the anatase nanotubes forms the interface junction[39,47] and thus a space-charge layer which expedites electron-hole separation. Besides, compared with nanotubes, the rutile nanorods/nanocrystals transport holes more efficiently to the semiconductor-liquid interface for water oxidation which minimizes recombination losses.

To support the above statement, photoluminescence (PL) measurements were further used to investigate the electron-hole recombination process in TiO_2 electrodes.[48,49] When a material is irradiated with light of appropriate wavelength, it generates electron-hole pairs, and then electron-hole pairs undergo a recombination process, finally photos are emitted, resulting in PL.[50] As shown in Fig. 5d, the PL spectra show that the samples have a broad-band emission. In comparison with pristine anatase TiO_2 nanotubes, the PL intensity of the hybrid TiO_2 nanostructures after hydrothermal treatment is much lower although the latter can absorb more light, which indicates a reduced charge carrier recombination because of the formation of interface junction between anatase nanotubes and rutile nanorods and nanocrystals.

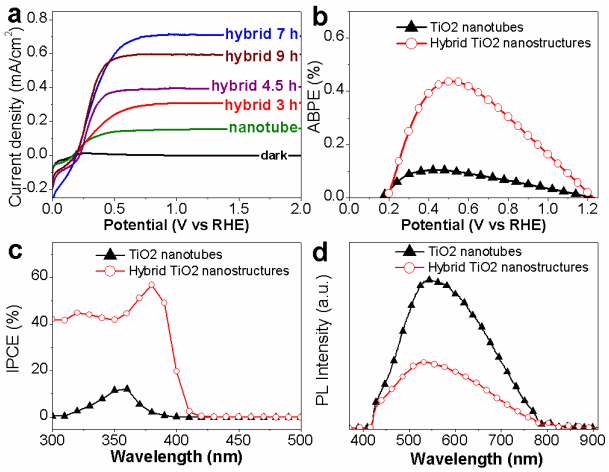

Fig. 5 (a) Measured photocurrent density as the applied potential (vs RHE) varies for TiO_2 nanotubes and hybrid TiO_2 nanostructures after 3 h, 4.5 h, 7 h, 9 h hydrothermal treatment, showing the enhanced photocurrent after hydrothermal treatment in comparison with pristine nanotubes. (b) ABPE of the TiO_2 nanotubes and hybrid TiO_2 nanostructures as a function of applied potential. (c) IPCE spectra of TiO_2 nanotubes and hybrid TiO_2 nanostructures at 0.23 V vs Ag/AgCl. (d) Room temperature PL spectrum of pristine TiO_2 nanotubes and hybrid TiO_2 nanostructures after hydrothermal treatment for 6h.

Conclusions

To summarize, hybrid TiO_2 nanostructures consisting of anatase TiO_2 nanotubes and rutile nanorods on the top of nanotubes (and also nanocrystals on the tube walls) were synthesized by hydrothermal treatment of anodized TiO_2 nanotubes. The photocurrent density and ABPE (under AM 1.5G illumination) of the hybrid TiO_2 nanostructures reached 0.71 mA/cm^2 and 0.45%, respectively, in comparison with 0.16 mA/cm^2 and 0.11% for pristine anatase TiO_2 nanotubes. For the hybrid TiO_2 nanostructures, the enhancement of photoactivity is a direct consequence of the synergistic effect of the growth of rutile nanorods/nanocrystals on anatase nanotubes, which expedites electron-hole separation and transportation, increases the surface area, and also enhances the light absorption. The conversion efficiency could be further

boosted by combining the mixed-phase one-dimensional TiO_2 nanostructures with material optimization by e.g. doping.

Acknowledgements

This work was supported in part by research grants from NSFC (61204074 and 91233208), Guangdong Innovative Research Team Program (201001D0104799318), and Department of Education of Guangdong Province. We thank Y.X. Zhao for his assistance in PL measurement.

Notes and references

[a] Centre for Optical and Electromagnetic Research,
South China Academy of Advanced Optoelectronics,
South China Normal University,
Guangzhou 510006, China.
E-mail: wnbn.huang@foxmail.com; optixy@foxmail.com

1. A. Fujishima and K. Honda, *Nature*, 1972, **238**, 37.
2. A. Kudo and Y. Miseki, *Chem. Soc. Rev.*, 2009, **38**, 253-278.
3. X. Chen, S. Shen, L. Guo and S. S. Mao, *Chem. Rev.*, 2010, **110**, 6503-6570.
4. F. X. Xiao, J. Miao, H. B. Tao, S. F. Hung, H. Y. Wang, H. B. Yang, J. Chen, R. Chen and B. Liu, *Small*, 2015.
5. X. Wang, K.-Q. Peng, Y. Hu, F.-Q. Zhang, B. Hu, L. Li, M. Wang, X.-M. Meng and S.-T. Lee, *Nano Lett.*, 2013, **14**, 18-23.
6. K. Zhu, N. R. Neale, A. Miedaner and A. J. Frank, *Nano Lett.*, 2007, **7**, 69-74.
7. G. K. Mor, K. Shankar, M. Paulose, O. K. Varghese and C. A. Grimes, *Nano Lett.*, 2006, **6**, 215-218.
8. K. Yu, X. Lin, G. Lu, Z. Wen, C. Yuan and J. Chen, *RSC Advances*, 2012, **2**, 7843-7848.
9. F. Li and X. Li, *Appl. Catal., A*, 2002, **228**, 15-27.
10. B. Liu, H. M. Chen, C. Liu, S. C. Andrews, C. Hahn and P. Yang, *J. Am. Chem. Soc.*, 2013, **135**, 9995-9998.
11. R. Asahi, T. Morikawa, T. Ohwaki, K. Aoki and Y. Taga, *science*, 2001, **293**, 269-271.
12. T. Ohno, T. Mitsui and M. Matsumura, *Chem. Lett.*, 2003, **32**, 364-365.
13. D.-L. Shieh, Y.-S. Lin, J.-H. Yeh, S.-C. Chen, B.-C. Lin and J.-L. Lin, *Chem. Commun.*, 2012, **48**, 2528-2530.
14. Y. Gao, Y. Feng, B. Zhang, F. Zhang, X. Peng, L. Liu and S. Meng, *RSC Advances*, 2014, **4**, 16992-16998.
15. G. Wang, H. Wang, Y. Ling, Y. Tang, X. Yang, R. C. Fitzmorris, C. Wang, J. Z. Zhang and Y. Li, *Nano Lett.*, 2011, **11**, 3026-3033.

16. J. Li, J. Zhang, L. Fang, J. Wang, M. Shen and X. Su, *J. Mater. Chem. A*, 2015, **3**, 4903-4908.
17. M. Liu, N. d. L. Snapp and H. Park, *Chem. Sci.*, 2011, **2**, 80-87.
18. K. Sivula, F. Le Formal and M. Gratzel, *ChemSusChem*, 2011, **4**, 432.
19. H.-E. Cheng, S. Hsiao and D.-M. Lu, *Electrochem. Solid-State Lett.*, 2010, **13**, D19-D22.
20. Y. J. Hwang, A. Boukai and P. Yang, *Nano Lett.*, 2008, **9**, 410-415.
21. J. Shi, Y. Hara, C. Sun, M. A. Anderson and X. Wang, *Nano Lett.*, 2011, **11**, 3413-3419.
22. G. K. Mor, K. Shankar, M. Paulose, O. K. Varghese and C. A. Grimes, *Nano Lett.*, 2005, **5**, 191-195.
23. J. H. Park, S. Kim and A. J. Bard, *Nano Lett.*, 2006, **6**, 24.
24. I. S. Cho, Z. Chen, A. J. Forman, D. R. Kim, P. M. Rao, T. F. Jaramillo and X. Zheng, *Nano Lett.*, 2011, **11**, 4978-4984.
25. X. Feng, K. Shankar, O. K. Varghese, M. Paulose, T. J. Latempa and C. A. Grimes, *Nano Lett.*, 2008, **8**, 3781-3786.
26. B. Liu and E. S. Aydil, *J. Am. Chem. Soc.*, 2009, **131**, 3985-3990.
27. Z. Zhang and P. Wang, *Energy Environ. Sci.*, 2012, **5**, 6506-6512.
28. X. Ao, X. Tong, D. S. Kim, L. Zhang, M. Knez, F. Müller, S. He and V. Schmidt, *Appl. Phys. Lett.*, 2012, **101**, 111901.
29. S. Wang, Z. Zheng, B. Huang, Z. Wang, Y. Liu, X. Qin, X. Zhang and Y. Dai, *RSC Advances*, 2013, **3**, 5156-5161.
30. R. Rahal, A. Wankhade, D. Cha, A. Fihri, S. Ould-Chikh, U. Patil and V. Polshettiwar, *RSC Advances*, 2012, **2**, 7048-7052.
31. R. I. Bickley, T. Gonzalez-Carreno, J. S. Lees, L. Palmisano and R. J. Tilley, *J. Solid State Chem.*, 1991, **92**, 178-190.
32. T. Kawahara, Y. Konishi, H. Tada, N. Tohge, J. Nishii and S. Ito, *Angewandte Chemie*, 2002, **114**, 2935-2937.
33. D. C. Hurum, A. G. Agrios, K. A. Gray, T. Rajh and M. C. Thurnauer, *J. Phys. Chem. B*, 2003, **107**, 4545-4549.
34. M. Ye, D. Zheng, M. Lv, C. Chen, C. Lin and Z. Lin, *Adv Mater*, 2013, **25**, 3039-3044.
35. J. Li, M. W. Hoffmann, H. Shen, C. Fabrega, J. D. Prades, T. Andreu, F. Hernandez-Ramirez and S. Mathur, *J. Mater. Chem.*, 2012, **22**, 20472-20476.
36. Y. K. Kho, A. Iwase, W. Y. Teoh, L. Mädler, A. Kudo and R. Amal, *J. Phys. Chem. C*, 2010, **114**, 2821-2829.
37. A. Testino, I. R. Bellobono, V. Buscaglia, C. Canevali, M. D'Arienzo, S. Polizzi, R. Scotti and F. Morazzoni, *J. Am. Chem. Soc.*, 2007, **129**, 3564-3575.
38. G. Li, S. Ciston, Z. V. Saponjic, L. Chen, N. M. Dimitrijevic, T. Rajh and K. A. Gray, *J. Catal.*, 2008, **253**, 105-110.
39. X. Zhang, Y. Lin, D. He, J. Zhang, Z. Fan and T. Xie, *Chem. Phys. Lett.*, 2011, **504**, 71-75.
40. P. Sun, X. Zhang, C. Wang, Y. Wei, L. Wang and Y. Liu, *J. Mater. Chem. A*, 2013, **1**, 3309-3314.
41. B. Liu, Y. Sun, X. Wang, L. Zhang, D. Wang, Z. Fu, Y. Lin and T. Xie, *J. Mater. Chem. A*, 2015.
42. J. Xu, J. Jin, Z. Ying, W. Shi and T. Peng, *RSC Advances*, 2015.
43. P. Zhao, P. Cheng, B. Wang, S. Yao, P. Sun, F. Liu, J. Zheng and G. Lu, *RSC Advances*, 2014, **4**, 64737-64743.

44. H. E. Prakasam, K. Shankar, M. Paulose, O. K. Varghese and C. A. Grimes, *J. Phys. Chem. C*, 2007, **111**, 7235-7241.
45. C. T. Yip, H. Huang, L. Zhou, K. Xie, Y. Wang, T. Feng, J. Li and W. Y. Tam, *Adv. Mater.*, 2011, **23**, 5624-5628.
46. D. Hurum, A. Agrios, S. Crist, K. Gray, T. Rajh and M. Thurnauer, *J. Electron. Spectrosc. Relat. Phenom.*, 2006, **150**, 155-163.
47. H. Wang, X. Tan and T. Yu, *Appl. Surf. Sci.*, 2014, **321**, 531-537.
48. K. Fujihara, S. Izumi, T. Ohno and M. Matsumura, *J. Photochem. Photobiol., A*, 2000, **132**, 99-104.
49. M. Anpo, M. Tomonari and M. A. Fox, *J. Phys. Chem.*, 1989, **93**, 7300-7302.
50. N. Zhang, S. Liu, X. Fu and Y.-J. Xu, *J. Phys. Chem. C*, 2011, **115**, 9136-9145.